Fusion Engineering and Design 228 (2026) 115760

Contents lists available at ScienceDirect

Fusion Engineering and Design

journal homepage: www.elsevier.com/locate/fusengdes

Theoretical background for a fast flow liquid metal divertor experiment

A. Vorobev [a,*], S. Smolentsev [b], A. Khodak [c], D. Gupta [c], D. Suarez [d], D. O'Dea [e], G. Stoneham [a], A. Shone [e], K. Moshkunov [a]

[a] Tokamak Energy Ltd, UK
[b] Oak Ridge National Laboratory, USA
[c] Princeton Plasma Physics Laboratory, USA
[d] University of Tennessee, Knoxville, USA
[e] Tokamak Energy Inc, USA

ARTICLE INFO

Keywords:
Liquid metal divertor
Fast flow concept
Liquid lithium
Experiment
Modelling
Fusion device

ABSTRACT

Tokamak Energy has developed a liquid metal experiment featuring a lithium loop that circulates lithium through the HIDRA stellarator at the University of Illinois at Urbana-Champaign. The loop includes a replaceable divertor module, designed to demonstrate fast, steady, open-surface liquid metal flow. The first-generation divertor module was deliberately kept simple—an open-surface chute—to enable modelling validation and establish a benchmark for future design iterations. This paper presents the theoretical foundations of the experimental design. Specifically, we identify module overflooding as the primary challenge and determine the limits of fluid velocity and magnetic field strength necessary to prevent it. The steady-state flow patterns are expected to exhibit relatively slow surface velocities, which do not fully align with the fast-flow concept. Nevertheless, the experiment is designed to achieve controllable, continuous open-surface flow within an operational fusion device, representing a significant step toward the development of liquid metal divertor technology.

1. Introduction

1.1. Motivation. Low-recycling concept

In a fusion device based on magnetic confinement, a divertor is a specialized plasma-facing component designed to perform an exhaust function. It addresses several key issues, including (i) removal of cold plasma and impurity particles from a fusion device, and (ii) removal of intense heat and sputtering loads on solid walls associated with the plasma beam that is redirected from the plasma core.

Liquid lithium is regarded as one of the most effective media for addressing these issues [1,2]. First, its strong capacity to absorb hydrogen isotopes suppresses the recycling of cold particles striking the divertor plate, reduces the accumulation of low-energy (including neutral) particles in the divertor zone, and prevents cooling at the plasma edge. Second, because lithium has a low atomic number, relatively high concentrations are required to significantly affect plasma properties when sputtered or evaporated from the divertor surface.

The absorption-based concept, known as the low-recycling concept, relies on slowly moving, thin lithium layers. In such layers, magnetohydrodynamic effects are less significant; however, surface-tension and wetting instabilities continue to govern the behaviour of the thin film. The low-recycling concept has been experimentally investigated in an operational fusion device [3], where observations confirmed the beneficial influence of lithium on plasma quality and the improvement of plasma confinement time. Direct observation of the film characteristics during the experiment was not possible, and subsequent analysis indicated incomplete wetting of the experimental plate. Moreover, increased flow rates during the experiment led to the ejection of lithium droplets, which in turn caused plasma disruptions.

The solution based on slow flow does not directly address the heat challenges of the divertor; instead, it relies on alternative approaches, such as detaching the plasma beam from the divertor plate by injecting neutral gas and cooling the plate with helium or another suitable fluid.

1.2. Fast flow concept. Flow speed

The heat challenge, along with the low-recycling challenge, can be

* Corresponding author.
E-mail address: anatoliy.vorobev@tokamakenergy.com (A. Vorobev).

https://doi.org/10.1016/j.fusengdes.2026.115760
Received 22 December 2025; Received in revised form 2 March 2026; Accepted 30 March 2026
Available online 4 April 2026

effectively addressed by liquid lithium flow, provided the flow is sufficiently fast and the layer sufficiently thick. This approach, known as the fast-flow concept [4], assumes that the heat from the plasma beam is carried away by the liquid flow, thereby achieving complete separation between the plasma and the solid wall.

For this concept to work, heat transfer in the flowing liquid lithium must be dominated by forced convection, i.e., the convective time (L/U) must be shorter than the thermal conduction time $\left(h^2/\chi\right)$. In other words, the flow speed must satisfy the condition

$$U > L\chi/h^2, \tag{1}$$

where L is the length of the protected surface, h is the thickness of the liquid layer, and $\chi = 2{\cdot}10^{-5}\,\mathrm{m}^2/\mathrm{s}$ is the thermal diffusivity of lithium.

Namely, to protect a full divertor of size $L \sim 1\,\mathrm{m}$, a liquid layer of thickness $h = 5\,\mathrm{mm}$ moving at an average speed of approximately $1\,\mathrm{m}/\mathrm{s}$ is required. If the liquid layer is thicker, the necessary flow speed can be lower. Conversely, a very thin layer is effectively transparent to the plasma heat flux, making realization of such a flow impossible. A localized solution, focused on the narrow plasma beam, would also relax the requirement on flow speed.

Additionally, let us examine whether the proposed fluid flow can deal with the expected heat loads of the plasma beam. When heat transfer is dominated by convection, the heat carried away by the flow is given by

$$Q = \dot{m} c_p \Delta T. \tag{2}$$

Here, $Q \approx q\lambda W$ represents the thermal heat flow rate deposited by the plasma beam, where q is the heat flux, λ is the thickness of the plasma beam, and W is the width of the divertor plate (or the perimeter in the case of a toroidally symmetrical divertor). The mass flow rate can be expressed as

$$\dot{m} = \rho U h W, \tag{3}$$

where ρ is the density of the liquid, U is the average flow velocity, and h is the thickness of the liquid layer. The heat capacity of the liquid is denoted by c_p, and ΔT represents the “temperature window,” i.e., the allowable temperature difference across the liquid layer.

The temperature window is determined by two factors [5]. First, hotter liquid exhibits higher evaporation rates, which may lead to plasma dilution. It is generally assumed that the temperature of lithium must remain below 450 °C to keep evaporation under control. Second, the liquid temperature must stay above the ductile-to-brittle transition temperature of the solid substrate. For RAFM steel, this transition occurs at 350 °C [6]; for vanadium alloy, at 400 °C [7]; for tungsten, at 600 °C, and for K-doped tungsten, at approximately 300 °C [8]. Consequently, pure tungsten cannot be used to construct the divertor wall if fast lithium flow is employed to cool the divertor surface. The other materials are suitable, and the choice of a specific material would define the temperature window.

By combining the above equations, one finds that the average velocity of the flow film must satisfy

$$U \approx \frac{q}{\rho c_p \Delta T}\frac{\lambda}{h}. \tag{4}$$

Assuming $q = 10\,\mathrm{MW}/\mathrm{m}^2$ and $\lambda = 1\,\mathrm{cm}$ (which do not correspond to any particular device but could be achieved with current devices [9]), $\rho = 500\,\mathrm{kg}/\mathrm{m}^3$, $c_p = 4200\,\mathrm{J}/(\mathrm{kg{\cdot}K})$, $\Delta T = 50\,\mathrm{K}$, and $h = 5\,\mathrm{mm}$, the result is $u \approx 1\,\mathrm{m}/\mathrm{s}$. This value is consistent with the earlier requirement that convection should dominate over thermal conduction. It should also be noted that this value represents the lower bound for the required fluid velocity (see [4]), appropriately so, since Eq. (4) provides only a rough estimate and because the actual heat flux can reach as high as $q = 50\,\mathrm{MW}/\mathrm{m}^2$ [9].

1.3. Fast flow experiments. Review of experimental observations

The fast-flow concept was first proposed in the 1970s in the Soviet Union (see, e.g., [10,11]). Since then, it has been investigated theoretically and experimentally by various research groups using different experimental setups: different working liquids (most commonly Galinstan, though a few experiments were also conducted with liquid lithium); varying inclination angles (typically relatively small, <9°, due to the substantial surface instability of film flows at higher angles); experimental chutes manufactured using electrically conductive and non-conductive materials; both with and without magnetic fields, applied at varying strengths (up to 5 T) and orientations (mostly spanwise, although the effects of streamwise and plate-normal components were also studied).

In fact, the structure and stability of thin-film, open-surface flows along solid walls are classical problems in fluid mechanics, many aspects of which are already well understood (see, e.g., [12]). This knowledge has been partially applied to fusion-relevant configurations. However, unlike the slow-flow concept, fast-flow experiments have not yet been carried out in an operational fusion device.

Based on prior experimental studies, the following issues have been identified:

- When fluid is pushed onto the plate, the flow transitions from a jet (or, an inertia-driven flow) to an established gravity-driven flow. Without a magnetic field, the test rigs are typically too small for this transition to be completed (e.g., [13]). However, if the fluid is not pushed but rather supplied through a long nozzle inclined at the same angle as the experimental plate, a fully developed gravity-driven flow can be sustained across the entire surface [14,15]. Under a strong magnetic field, the transition occurs much more rapidly and is largely confined to the vicinity of the nozzle (see, e.g., [13]).
- In the absence of magnetic field, the flow is usually turbulent, exhibiting a complex, wavy surface pattern (e.g. [13,15]), which evolve along the surface, with varying amplitudes, wavenumbers, and wave structures (e.g., [16]).
- The thickness of the film flow typically changes along the chute. Even without a magnetic field, open-surface flows often exhibit hydraulic jumps, where the liquid layer suddenly thickens and the flow decelerates (e.g., [17,18]).
- In the absence of a magnetic field, the flow pattern on a wide chute is symmetric about the centreline, with noticeable deceleration near the side walls (e.g., [13,15,17]). At low flow rates, however, the liquid may fail to cover the entire surface, instead forming rivulets (e.g., [12,18]).
- The influence of the magnetic field strongly depends on its orientation. When aligned parallel to the surface and normal to the side walls, the field laminarizes the flow and suppresses surface waves (e.g., [16]); however, its impact on other flow characteristics is moderate. When oriented perpendicular to the bottom plate, the field not only laminarizes but also strongly slows the fluid, causing significant accumulation of the fluid on the chute (e.g., [17]). Furthermore, a magnetic field normal to the bottom plate induces three-dimensional flow instabilities, resulting in a “wavy” (asymmetric) pattern with possible detachment of the liquid from side walls (e.g., [17,19]).
- The influence of the magnetic field strongly depends the electrical conductance of the walls [20].
- Forced pre-wetting of the chute is required to initiate flow with a good surface coverage (see, e.g., [15,16]). Under strong temperature variations on the bottom plate, thermocapillary instabilities may also develop (e.g., [12]).
- Observations have also been made during inductive plasma initiation and termination at the start and end of a tokamak pulse, which involve rapid changes in the magnetic field. These studies demonstrated ejection of droplets from the open surface (e.g., [21]).

2. Problem statement

2.1. HIDRA stellarator. Parameters of the new experiment

At Tokamak Energy, we aim to investigate the fast-flow concept using a small-scale lithium loop that integrates a test module within the HIDRA stellarator, a research fusion device located at the University of Illinois Urbana-Champaign.

The initial objective is to achieve a fast lithium flow with good substrate coverage and to investigate the influence of the magnetic field on the flow characteristics. In this study, the flow will be assumed isothermal. While we justify the need for a fast flow based on heat-removal considerations, the (plasma) heat load itself will not be part of the first experimental stage. Joule heating is assumed to be absorbed and dissipated by the structural components and is therefore disregarded in our analysis. The experimental module will include heating elements designed to control the substrate temperature. In addition, the loop will incorporate heating elements to maintain a uniform lithium temperature throughout the system.

The dimensions of HIDRA—particularly its minor radius of 19 cm—play a significant role in shaping the experimental setup. Fig. 1 shows the experimental set up. The loop consists of a lithium loading chamber, a storage reservoir, and two pipelines equipped with moving magnet pumps that transport lithium to and from the experimental module. The pumps can sustain flow rates of up to 400 g/s. Vacuum conditions are maintained within both the stellarator and the storage reservoir. The experimental module is positioned at the highest point of the loop, enabling complete removal of lithium from the stellarator at the end of the experiment.

The experimental module comprises a compression nozzle, an experimental chute (open-surface flow region), and a collector. The nozzle gap height is 3 mm. Although the collector has a complex shape, its surface area is larger than that of the nozzle. Several variations of the collector design were evaluated, with the collector's cross-sectional flow area exceeding that of the nozzle by a factor of 1.7–2.

The experimental plate is relatively wide, measuring 9.25 cm in length and 7.5 cm in width. Its inclination angle is 5°, and the side walls are 2.95 cm high. The plate will be manufactured from stainless steel SS316 with a thickness of 11 mm.

The experimental module is installed inside the stellarator, which is equipped with both toroidal and helical magnets, and the currents in the magnet coils can be independently controlled. The maximum steady magnetic field achievable at the maximum coil currents is shown in Fig. 2.

The magnetic field is characterized by three components, but in Fig. 2, we present two of them: the toroidal component B_t, which is tangential to the plate and perpendicular to the flow direction, and the plate-normal component B_n, which is perpendicular to the plate. The toroidal component has a greater magnitude (>0.5 T) and varies slightly

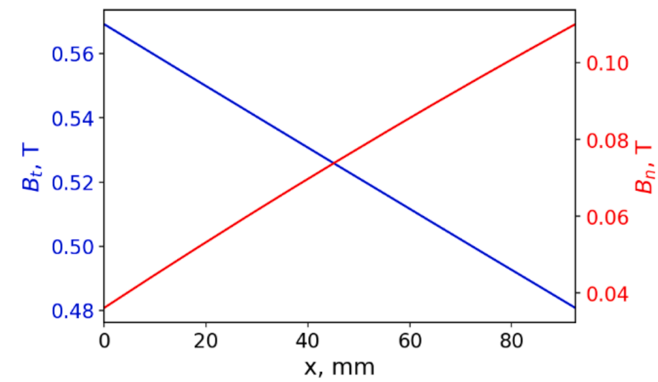

Fig. 2. The toroidal and plate-normal components of the magnetic field along the midplate.

along the plate. In contrast, the plate-normal component undergoes nearly a three-fold change along the plate, with its maximum value exceeding 0.1 T

2.2. The effect of the toroidal and plate-normal components of the magnetic field

The magnetic field expected in a commercial fusion device, which could serve as the foundation for a fusion power plant, will be substantially stronger. An advantage of the current experiment is the ability to shape the magnetic field into different configurations, and to assess the effect of the plate-normal component on the flow. For a divertor, the plate-normal component is essential, as it directs the plasma beam toward the divertor plate. In fact, the presence of a non-zero plate-normal component is one of the key differences distinguishing the design of a liquid metal first wall from that of a liquid metal divertor.

There are several ideas for implementing the fast-flow solution in the design of a fusion device. One option that may seem easier to realize is the sectioned design, in which the divertor plate is replaced by a chute shaped similarly to our experimental module. The major drawback of this approach is that it provides only a partial solution to the heat load, since each chute has solid side walls that remain exposed to the plasma beam. A more promising option appears to be a toroidally symmetrical divertor; however, the toroidally symmetrical design may introduce maintenance challenges and could allow toroidal currents in the divertor region that may interfere with plasma control measures. Furthermore, in a toroidally symmetrical design, the liquid may be exposed to the high heat flux zone for a longer duration, as the flow tends to follow the magnetic field lines, which follow a spiral rather than a radial direction.

In a toroidally symmetrical divertor, only the plate-normal

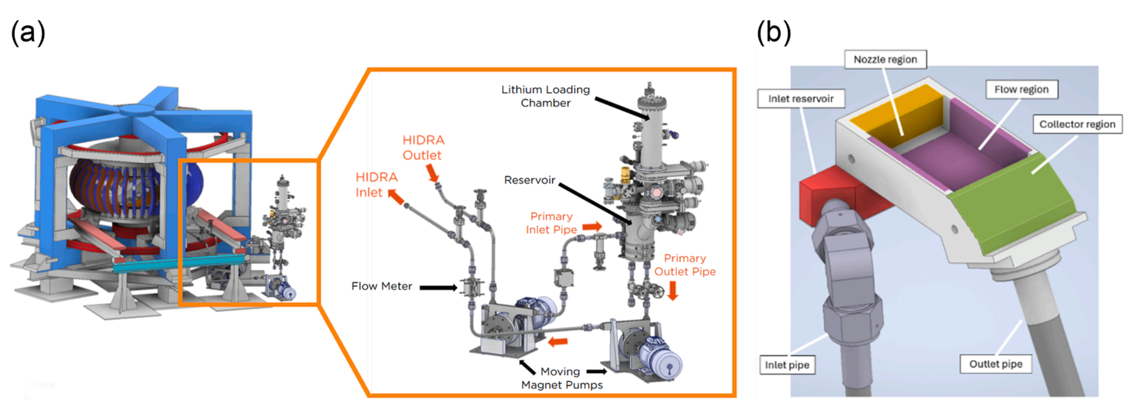

Fig. 1. (a) HIDRA stellarator with the lithium loop; (b) Replaceable experimental module.

component influences the flow. In a sectioned divertor, both the toroidal and plate-normal components can contribute. However, the influence of the toroidal component is confined to the wetted area of the side walls (where the Hartmann layers are formed), while the effect associated with the plate-normal component spreads over the entire substrate area (where the Hartmann layer is formed in this case). Hence, for wide chutes and thin films, the effect of the plate-normal component can become dominant.

Indeed, the ratio between the braking forces induced by these two components can be estimated as $\sim \frac{h_0}{W}\left(\frac{B_t}{B_n}\right)^2$, where $\frac{h_0}{W}$ is the ratio of the layer thickness to the plate width. This estimate follows the classical fitting equation for the MHD pressure drop in a duct with a rectangular cross-section [22]. It is well established that for a duct with wall dimensions a and b, and wall conductance κ, the pressure drop (or equivalently, the Lorentz force) is given by $-\frac{dp}{dx} = k_p \sigma U B^2$, where $k_p = \frac{\kappa}{1+a/3b+\kappa}$. For a toroidal magnetic field, $a = W$ and $b = h_0$, so $a/b \gg 1$, and the force per unit volume is approximately $f_t \sim \frac{h_0}{W}\sigma U B_t^2$. In contrast, for a plate-normal magnetic field, $a/b \ll 1$, and the force is approximately $f_n \sim \sigma U B_n^2$. The ratio of these two expressions provides a rough guideline for comparing the braking effects induced by toroidal and plate-normal magnetic fields. A similar observation is reported in [23], where the influence of the toroidal magnetic field on the chute flow is analysed.

In this work, the effect of the plate-normal component on the flow down the plate is the major focus, although the influence of the toroidal component will be also discussed.

The effect of the magnetic field is traditionally characterised by the Hartmann number. We can introduce two Hartmann numbers,

$$Ha_t = W B_t \sqrt{\frac{\sigma}{\eta}} \text{ and } Ha_n = h_0 B_n \sqrt{\frac{\sigma}{\eta}}, \tag{5}$$

to characterise the effects of the toroidal and plate-normal magnetic fields, respectively. Here, $\sigma = 3{\cdot}10^6$ S/m is the lithium electrical conductivity and $\eta = 5{\cdot}10^{-4}$ Pa·s is its dynamic viscosity [24]. Assuming, $B_t = 0.5$T, and $B_n = 0.05$T, the parameters of this experiment yield $Ha_t \approx 2900$ and $Ha_n \approx 12$.

2.3. A developing flow

To understand the characteristics of liquid metal flow along an inclined plate, let us start with a 2D analysis (as illustrated in Fig. 3), assuming that the plate is sufficiently wide ($\frac{h_0}{W} \ll 1$) so that the effects of the side walls can be neglected. The magnetic field is considered to have only one component—normal to the plate—which remains uniform along its length.

We assume that the liquid is injected onto the plate with an initial velocity (hence also referred as a "jet"), forming a film flow whose initial thickness is determined by the nozzle gap. For the parameters of interest here ($U_0 \approx 1$ m/s and $h_0 = 3$ mm), the Reynolds number of the flow near the nozzle, $Re = \frac{U_0 h_0}{\nu} \approx 3000$, where $\nu = 10^{-6}$ m^2/s is the viscosity of lithium, is considerably higher than the critical Reynolds number that defines the onset of surface instability for a film flow, $Re_c = \frac{5}{6}\cot\beta \approx 9.5$, with $\beta = 5°$ being the plate's inclination angle [25]. Hence, in the absence of a magnetic field, the flow will be turbulent and exhibit a complex surface shape. However, it is well established that a magnetic field can suppress surface instabilities, or at least reduce their growth rate [26].

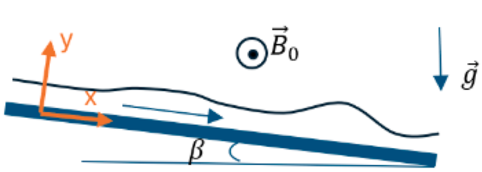

Fig. 3. A film flow down an inclined plate.

The flow down an inclined plate is likely governed by different physical mechanisms at varying distances from the nozzle. The inertia-driven flow, characterized by average velocity and thickness defined by the inlet conditions, gradually transforms into gravity-driven flow. This transition occurs as information about the open-surface boundary conditions propagates into the bulk of the layer, accompanied by a corresponding adjustment of the viscous friction force. In the absence of a magnetic field, the plate length required for the transition to complete can be roughly estimated by comparing the inertial and viscous terms in the Navier–Stokes equation. This estimate is given as $L_{\text{no-magn}} \sim \frac{U_0 h_0^2}{\nu}$ (which can be also interpreted as the product of the average velocity and the typical hydrodynamic time). This estimated length is substantially greater than that of the experimental plate ($L_{\text{no-magn}} = 9$m, if $U_0 \sim 1$m/s, $h_0 = 3$mm and $\nu = 10^{-6}$m^2/s), a conclusion supported by numerous experimental observations (e.g. [13]).

However, if a magnetic field is applied, the transition can be expected to occur over a shorter flow path. For a plate with good electrical conductivity (as in our experiment), the length required for the full transition can be estimated by comparing the inertial and Lorentz forces. The estimate is given as $L_{\text{magn}} \sim \frac{1}{Ha_n^2}{\cdot}\frac{U_0 h_0^2}{\nu}$ (the product of the average velocity and the braking time $\frac{1}{Ha_n^2}{\cdot}\frac{h_0^2}{\nu}$ [25]). This estimated length is already smaller than the length of the experimental plate ($L_{\text{magn}} = 6$cm if $U_0 \sim 1$m/s, $h_0 = 3$mm and $Ha_n \approx 12$). Hence, in the presence of a magnetic field, the transition from inertia-driven to gravity-driven flow occurs within the experimental plate a result also confirmed by the experiments (e.g. [13]).

Additionally, because we are interested in the characteristics of the steady-state flow, the backward influence of the collector's capacity on the flow may also be important, which will be discussed later.

The initial distribution of liquid on the chute can vary, so it is important to ensure full wetting of the chute's internal surface before the experiment begins. One option is to take advantage of the relatively small inclination angle: close the outlet valve, flood the chute, and then initiate throughput flow. Another option is to exploit the dependence of wetting conditions on wall temperature [28] by preheating the plate to, for example, 500 °C at the start of the experiment (with heating elements incorporated into the plate). In this latter case, the initial temperature distribution may be non-uniform, which could complicate the flow; however, the incoming liquid will quickly render the temperature field uniform.

3. Analytical analysis

3.1. A developed gravity-driven flow. No magnetic field

The development of a jet flow on the chute is quite complex and would require numerical analysis (see, e.g., [27,29], and the analysis completed below). However, the features of an established gravity-driven flow are easier to comprehend. By applying mass conservation to correlate the characteristics of the gravity-driven flow with the inlet conditions, one may obtain a crude understanding of what the development of the jet flow might involve. For this purpose, let us now examine more closely the parameters governing the established gravity-driven flow. Here, for completeness, we provide the formulae for the cases with and without a magnetic field. It should be emphasized, however, that in the designed experiment the establishment of the established gravity-driven flow can be expected only when a magnetic field is applied.

In the absence of a magnetic field, the 2D laminar velocity profile of the steady-state flow is described by the classical expression commonly referred to as the "Nusselt solution",

$$u_x = \frac{\rho g \sin\beta}{\eta} y\left(h - \frac{1}{2}y\right). \tag{6}$$

Here g is the gravitational acceleration and y is the coordinate that is normal to the plate. We assume that the flow is unidirectional, unrestricted at the sides, and with a fixed thickness h. It is also convenient to write the expression for the mass flow rate,

$$\dot{m} = \rho W \frac{\rho g \sin\beta}{3\eta} h^3. \tag{7}$$

And, for the practical analysis, it is also convenient to express the average velocity ($U = \langle u_x \rangle = \frac{\dot{m}}{\rho W h}$) and the thickness of the gravity-driven flow in terms of the mass flow rate,

$$U = \left(\frac{\dot{m}}{\rho W}\right)^{2/3}\left(\frac{\rho g \sin\beta}{3\eta}\right)^{1/3} \text{ and } h = \left(\frac{\dot{m}}{\rho W}\frac{3\eta}{\rho g \sin\beta}\right)^{1/3}. \tag{8}$$

By applying Eqs. (7) and (8) to a purely gravity-driven film flow with a thickness of 3 mm, the resulting mass flow rate is 290 g/s, and the average velocity is 2.6 m/s. Thus, in the absence of a magnetic field, the gravity-driven flow of the expected thickness is substantially faster than the targeted inertia-driven flow (with a mean velocity of approximately 1 m/s). If the inlet velocity is lower than the value prescribed by Eq. (8), the liquid velocity must increase along the plate, and the layer thickness must decrease (provided the collector has sufficient capacity). However, as noted above, if the magnetic field is switched off, the full transition to gravity-driven flow regimes requires a considerable distance that is not available in the current experiment. Consequently, in the designed experiment, the liquid layer will simply maintain a (nearly) constant thickness.

3.2. A developed gravity-driven flow. With magnetic field

In the presence of magnetic field, the velocity profile (scaled by the average velocity $U_0 = \langle u_x \rangle$) is defined by

$$\frac{u_x}{U_0} = \frac{Ha_n}{Ha_n - \tanh Ha_n}\left(1 - \cosh\left(Ha_n\frac{y}{h}\right) + \tanh(Ha_n)\sinh\left(Ha_n\frac{y}{h}\right)\right). \tag{9}$$

The derivation of Eq. (9) is given in Appendix. It is straightforward to show that, in the limit of a strong magnetic field ($Ha_n \to \infty$), the velocity profile is uniform throughout the bulk of the layer, except within a thin Hartmann boundary layer of a thickness approximately equal to h/Ha_n, where the velocity rapidly adjusts to satisfy the no-slip boundary condition.

The expression for the flow profile does not depend on the plate's conductivity, but the flow rate does. Namely, the flow rate can be obtained from the following expression,

$$\frac{Fr^2}{Re} = \frac{\sin\beta}{Ha_n^2}\left(\frac{Ha_n}{Ha_n - \tanh Ha_n} - \frac{1}{1+\kappa}\right)^{-1}, \tag{10}$$

or, in the dimensional form,

$$U = \frac{\dot{m}}{\rho W h} = \frac{\rho g h^2 \sin\beta}{\eta} Ha_n^{-2}\left(\frac{Ha_n}{Ha_n - \tanh Ha_n} - \frac{1}{1+\kappa}\right)^{-1}. \tag{11}$$

Here $Fr = \frac{U_0}{\sqrt{g h_0}}$ is the Froude number. We also introduce the conductance that is defined as $\kappa = \frac{\sigma_w h_w}{\sigma h}$, where σ_w is the electrical conductivity of the wall material and h_w is the thickness of the wall. We should note that the experimental rig is made of stainless steel with $\sigma_w = 10^6$ S/m and $h_w = 11$mm, resulting in a relatively high conductance of $\kappa \approx 1.2$.

For weak magnetic fields ($Ha_n \to 0$) expression (11) produces the flow rate given by the Nusselt solution (6). For strong magnetic fields ($Ha_n \to \infty$), the flow rate strongly depends on the plate's conductance, so the corresponding expressions for the electrically insulating ($\kappa = 0$) and electrically conducting plates would differ,

$$U = \frac{\dot{m}}{\rho W h} = \frac{1}{Ha_n}\frac{\rho g h^2 \sin\beta}{\eta} \text{ and } U = \frac{\dot{m}}{\rho W h} = \frac{1}{Ha_n^2}\frac{1+\kappa}{\kappa}\frac{\rho g h^2 \sin\beta}{\eta}. \tag{12}$$

The magnitude of the Lorentz force depends on the currents generated by the flow. The current density is given by the expression

$$j_z = \sigma B_n\left(u_x - \frac{\kappa}{\kappa+1}U_0\right). \tag{13}$$

The electric currents flow in the z-(toroidal) direction.

Finally, let us re-write Eqs. (12) to derive the expressions for the average velocities and thicknesses of a gravity-driven flow in terms of the mass flow rate,

$$U = \frac{1+\kappa}{\kappa}\frac{\rho g \sin\beta}{\sigma B_n^2} \text{ and } U = \left(\frac{\dot{m}}{\rho W}\frac{\rho g \sin\beta}{\sqrt{\sigma\eta}B_n}\right)^{1/2} \tag{14}$$

$$h = \frac{Q}{\rho W}\frac{\kappa}{1+\kappa}\frac{\sigma B_n^2}{\rho g \sin\beta} \text{ and } h = \left(\frac{\dot{m}}{\rho W}\frac{\sqrt{\sigma\eta}B_n}{\rho g \sin\beta}\right)^{1/2}. \tag{15}$$

The first expressions in (14) and (15) describe flow along an electrically conductive plate, while the second expressions pertain to an electrically insulating plate. Notably, the average velocity of flow over a conductive plate is independent of the flow rate. In this case, the velocity is governed solely by the plate's inclination and by electromagnetic parameters. Increasing the fluid input at the upper end of the plate will only result in a thicker film, without affecting the speed of the film's movement.

For convenience, the dependencies of average velocity and layer thickness on the flow rate are shown in Fig. 4, providing quick and accessible guidance for understanding the values of these parameters in the experiment.[1]

Namely, in the absence of a magnetic field, or when the magnetic field is applied but the plate is electrically insulating, overflooding is unlikely. In these cases, we expect a transition from the initial jet flow with a thickness of 3 mm to a gravity-driven flow with a thickness indicated in Fig. 4b. Although this thickness may exceed 3 mm, it remains below the 2.95 cm limit set by the height of the side walls. However, if the plate is electrically conductive, the maximum allowable magnetic field strength is strongly constrained. This is additionally illustrated by Fig. 5, which depicts the maximum allowable mass flow rate before overflooding may occur in the experimental module. Specifically, if the plate-normal component of the magnetic field of 0.05 T and plate's conductance of 1.2, the maximum allowable mass flow rate is about 110 g/s.

3.3. Toroidal magnetic field. Effect of side walls

In the previous sections, the effect of a magnetic field imposed on the flow is attributed entirely to its normal component, which is explained by the fact that the influence of the toroidal magnetic field diminishes as the ratio $h/W \to 0$ (and in this experiment the chute is deliberately chosen wide). A detailed analysis of the effect of the toroidal magnetic field is presented in [23], where it is shown that the introduction of a magnetic field leads to flow deceleration and thickening of the fluid layer. When the chute's walls possess high electrical conductance, the magnetic field's effect becomes so pronounced that the film velocity becomes independent of the flow rate. In such cases, adding more fluid primarily results in a substantial increase in the layer's thickness.

The clear similarity between the effects induced by the plate-normal

[1] The average velocity does not vanish in the limit of zero mass flow rate, which is a non-physical result. This outcome arises from the assumption underlying Eqs. (12)–(15), namely that the Hartmann number is large and, consequently, the thickness of the Hartmann layer is much smaller than that of the main layer. At very low flow rates, however, this assumption clearly breaks down.

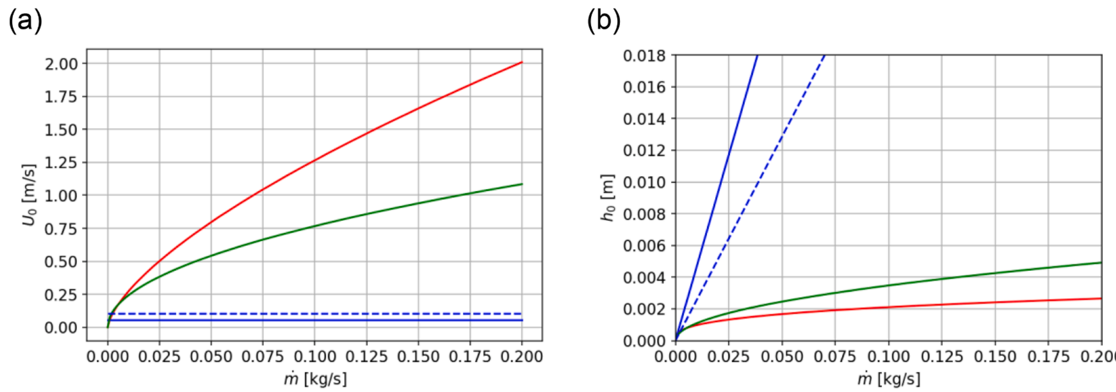

Fig. 4. The average velocity (a) and film thickness (b) for gravity-driven flow along an inclined plate are presented for three cases: when the magnetic field is switched off (red line), and when it is switched on, assuming an electrically insulating plate (green line) and a perfectly conducting plate (blue line) and the conductance of $\kappa = 1.2$ (blue dashed line). Here we assume that the plate's inclination is given by the angle of 5°, and the strength of the magnetic field is defined by $B_n = 0.05$T.

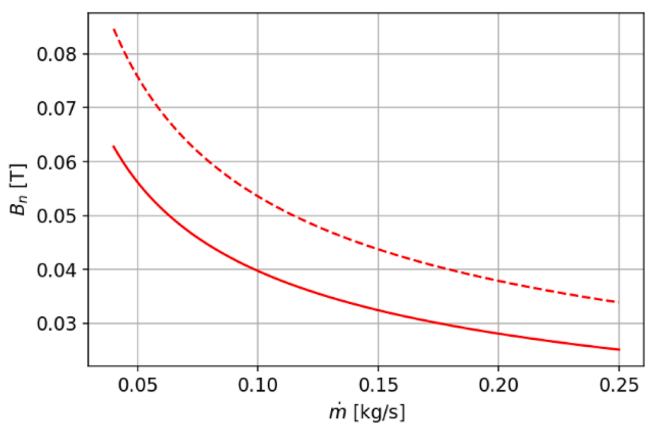

Fig. 5. Magnetic field strength versus the maximum allowable mass flow rate before overflooding occurs in the experimental module. The dashed line depicts the result for the plate's conductance of 1.2 and solid line for the perfectly conducting plate.

and toroidal magnetic fields suggests that, once the effect of the toroidal field is taken into account, the data shown in Figs. 4 and 5 should be regarded as an underestimation. Nevertheless, the qualitative behaviour predicted by Figs. 4 and 5 remains valid.

3.4. A gravity-driven flow with a slightly deformable open surface

A fully developed flow driven solely by gravity maintains a constant thickness in the liquid layer (disregarding surface waves). Such a flow is characterized by a specified flow rate (Eqs. (7) or (12)). In this section, we examine what happens when the throughput flow rate differs from that of the gravity-driven flow.

Let us consider a laminar film flow that is predominantly driven by gravity with a slightly deformable open surface. We consider a steady-state ($\frac{\partial}{\partial t} = 0$) flow of a thin fluid film assuming the flow remains nearly unidirectional ($u_x \gg u_y$, $\frac{\partial}{\partial x} << \frac{\partial}{\partial y}$), and the magnetic field is switched off. With these assumptions in place, one can derive the following expression for the pressure in the liquid layer,

$$p = \rho g(h - y)\cos\beta. \tag{16}$$

Here, $p(x)$and $h(x)$ denote the pressure and the thickness of the liquid layer, both of which may vary along the plate. From Eq. (16), it is evident that by pushing the fluid along the plate (creating an externally imposed pressure difference along the plate), one would also create a "pile-up," with the resulting gravitational force governing the fluid's motion along the plate. Thus, any open-surface flow—even flow on a horizontal plate—is ultimately always driven by gravity.

Namely, when fluid is actively pushed onto the plate, both pressure and film thickness vary along the surface, as predicted by the following equations:

$$\frac{\partial p}{\partial x} = \rho g\sin\beta - 3\frac{\eta U_0}{h_0^2} = \rho g\cos\beta\left(\tan\beta - \frac{3Fr^2}{Re\cos\beta}\right), \tag{17}$$

$$\frac{\partial h}{\partial x} = \tan\beta - \frac{3U_0\eta}{\rho g h_0^2\cos\beta} = \tan\beta - \frac{3Fr^2}{Re\cos\beta}. \tag{18}$$

Analysis of the above equations indicates that the shape of the liquid surface is primarily determined by the intensity of the throughput flow. In the absence of flow ($U_0 = 0$), the open surface remains horizontal, and consequently, the thickness of the liquid layer increases along the plate (see Fig. 6a). This state may represent the initial stage of the experiment, providing full wetting of the experimental chute.

A weak throughput flow results in a slight inclination of the liquid surface, while the film thickness increases along the plate, as schematically shown in Fig. 6b In this case, the motion is slowed by the distribution of the liquid on the plate that is "unfavourable" to the flow. This situation in fact corresponds to the experimental settings for the case of the flow in the absence of a magnetic field. For example, with a flow thickness of $h_0 = 3$ mm, a velocity of $U_0 \approx 1$ m/s, and a plate inclination of $\beta = 5°$, the Froude number is $Fr = 5.8$. Under these parameters, the film thickness gradient is positive, meaning that the thickness of the film increases along the plate.

When both gradients vanish (so the film thickness remains constant), the flow is governed solely by gravity (Fig. 6c). Finally, when the throughput velocity is relatively high, the film thickness decreases along the plate (Fig. 6d). In this case, stronger forcing of the fluid produces a "bump" near the nozzle, which converts the applied push into an enhanced gravitational effect, helping to sustain a faster flow.

Let us now analyse the expressions for the pressure and film thickness gradients when the (plate-normal) magnetic field is applied. In this case, the expressions analogous to (17) and (18) become

$$\frac{\partial p}{\partial x} = \rho g\cos\beta\left(\tan\beta - \frac{Fr^2 Ha_n^2}{Re\cos\beta}\left(\frac{Ha_n}{Ha_n - \tanh Ha_n} - \frac{1}{1+\kappa}\right)\right), \tag{19}$$

$$\frac{\partial h}{\partial x} = \tan\beta - \frac{Fr^2 Ha_n^2}{Re\cos\beta}\left(\frac{Ha_n}{Ha_n - \tanh Ha_n} - \frac{1}{1+\kappa}\right). \tag{20}$$

It is straightforward to show that when $\kappa = 0$ and $Ha_n \to \infty$ Eqs. (20) and (21) reduce to

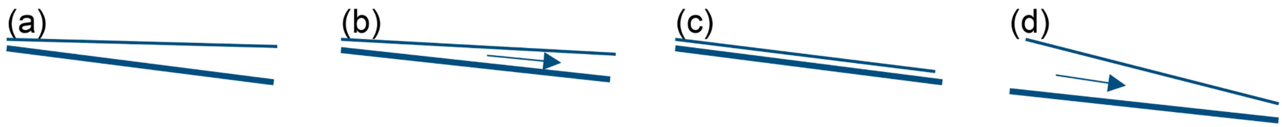

Fig. 6. Steady-state shapes of the open surface of a liquid film: (a) the liquid is at rest, with a horizontal open surface; (b) the liquid flows down the plate at low velocity; (c) the liquid motion is governed solely by gravity; (d) the liquid is pushed too strongly, producing a bump near the nozzle.

$$\frac{\partial p}{\partial x} = \rho g \sin\beta - B_n \frac{U_0}{h_0}\sqrt{\sigma\eta} = \rho g \cos\beta\left(\tan\beta - \frac{Fr^2 Ha_n}{Re\cos\beta}\right), \tag{21}$$

$$\frac{\partial h}{\partial x} = \tan\beta - \frac{B_n}{\rho g\cos\beta}\frac{U_0}{h_0}\sqrt{\sigma\eta} = \tan\beta - \frac{Fr^2 Ha_n}{Re\cos\beta}. \tag{22}$$

These two equations define the flow along an electrically insulating plate. Similarly, when $\kappa\to\infty$ and $Ha_n\to\infty$, Eqs. (19) and (20) reduce to equations:

$$\frac{\partial p}{\partial x} = \rho g \sin\beta - \sigma U_0 B_n^2 = \rho g\cos\beta\left(\tan\beta - \frac{Fr^2 Ha_n^2}{Re\cos\beta}\right), \tag{23}$$

$$\frac{\partial h}{\partial x} = \tan\beta - \frac{\sigma U_0 B_n^2}{\rho g\cos\beta} = \tan\beta - \frac{Fr^2 Ha_n^2}{Re\cos\beta}, \tag{24}$$

which work if the plate is a perfect conductor.

Using the above estimations of the Froude, Reynolds, and Hartmann numbers, one can readily observe that both the pressure and film thickness gradients are negative. This indicates that the fluid is forced onto the plate at a velocity higher than that of a gravity-driven flow, resulting in a pronounced “bump” near the nozzle (see Fig. 6d). In the case of a well conductive plate, the “bumping” effect is amplified by a factor of Ha_n.

Recall that the assumption in this section is that changes in the interface shape are small, which holds when the inlet flow characteristics closely match those of a purely gravity-driven flow (i.e., both $\partial p/\partial x \approx 0$ and $\partial h/\partial x \approx 0$). Achieving such alignment in an experiment is challenging, but certain features of the open-surface flow predicted by this simplified analysis should still be observed even when changes to the open surface are more pronounced. Specifically, if the throughput velocity is lower than that of the gravity-driven flow (which may be limited by a collector of inadequate capacity), fluid will begin to accumulate near the collector, forming a “bump” that regulates the rate of the gravity-driven flow. Conversely, if the throughput velocity exceeds that of the gravity-driven flow—meaning the fluid is supplied at a rate that cannot be sustained by gravity alone—a “bump” will instead form near the nozzle.

4. Numerical analysis

4.1. A layer of a fixed thickness

Next, we perform numerical modelling to support and extend the conclusions drawn from the 2D analytical analysis presented in the previous sections. The numerical simulations are conducted using two approaches. In this section, we present the results of 3D modelling of liquid metal flow along a chute, neglecting surface deformations and assuming laminar flow. Without a magnetic field, the flow becomes turbulent and exhibits pronounced surface waves; this case is not considered here. With a magnetic field applied, the flow remains laminar, though significant deformation of the free surface is expected. Here, however, we assume that the flow is still governed by the inlet conditions (inertia-driven flow) prior to the onset of strong deformation. The results obtained with this approach reproduce several phenomena observed in the experiments, which is why we consider it is important to present and discuss them.

Computations were performed using COMSOL and OpenFOAM using the quasi-static (inductionless) approximation of the full MHD equations. COMSOL images are shown below.

The numerical solutions were obtained using a uniform mesh in the x (streamwise) direction (with 20 grid-points) and non-uniform meshes with 160 grid points in the y (spanwise) direction and 80 points in the z (vertical) directions, with mesh refinement (typically by a factor of 2, but stronger refinement factors were also tested) near the walls. Test calculations with doubled resolution were carried out to confirm mesh independence of the results. The focus was primarily on obtaining the stationary solution.

For a more accurate representation of the plate’s inlet boundary conditions, the geometry includes a nozzle, modelled as a slotted duct with a height of 3 mm and a width of 7.5 cm. Although this geometry simplifies the nozzle shape used in the experiment, it provides a reasonable inlet velocity profile for the open-surface flow.

At the nozzle entrance, a uniform velocity profile with a flow speed of 1 m/s is assumed. A shear-stress-free boundary condition is applied at the free surface, while no-slip boundary conditions are enforced at all rigid walls. The outlet condition, defined as a zero-pressure level, is specified at the plate exit. Additionally, a zero normal component of the electric current density is imposed at the inlet and outlet boundaries, as well as at the open liquid surface. On the solid walls, the boundary conditions are either a fixed electrical potential (for perfectly conductive walls) or zero electric current density (for electrically insulating walls).

Fig. 7 provides the top views of the flows presented for three different magnetic field configurations. If the magnetic field is either purely toroidal or purely plate-normal, the velocity pattern is symmetric about the plate’s centreline. In the case of a toroidal magnetic field, at the plate’s entry the surface flow speed is lower near the centreline and higher at the sides. By the middle of the plate, however, the profile of the surface velocity becomes more uniform. For a plate-normal magnetic field, the flow profile remains uniform along the entire plate. When the magnetic field is inclined, the flow pattern becomes skewed: the surface velocity is greater for the liquid near one wall and slower next to the opposite wall. This asymmetry is likely to cause detachment of the fluid from the side wall, leading to the formation of a dry zone along one side of the chute [30].

The effect of the toroidal field is strong, particularly near the side walls. The affected zone extends far beyond the thickness of the Hartmann boundary layer. Even when the chute’s walls are electrically insulating, the electric vortices induced near the walls reach dimensions several times the boundary layer thickness. In the case of electrically conductive walls, the side effect also penetrates a distance of several layer thicknesses, substantially slowing the fluid flow near the side walls. This suppression of flow at the sides, due to mass conservation, results in an acceleration of the fluid flow in the middle of the plate.

Fig. 8 depicts the velocity and current density maps at the plate’s exit for chutes with different electrical conductivities of the walls. If the walls of the chute are electrically insulating, all electrical currents remain confined within the liquid domain. In contrast, with electrically conductive walls, the currents penetrate into the walls. For a toroidal magnetic field, electrical charges move from the bottom toward the sides of the walls, producing a symmetrical distribution of currents around the centreline. Under a plate-normal magnetic field, the currents flow from one side wall to the opposite side. When the magnetic field is inclined, the currents also move from the bottom toward the sides; however, their distribution becomes asymmetrical.

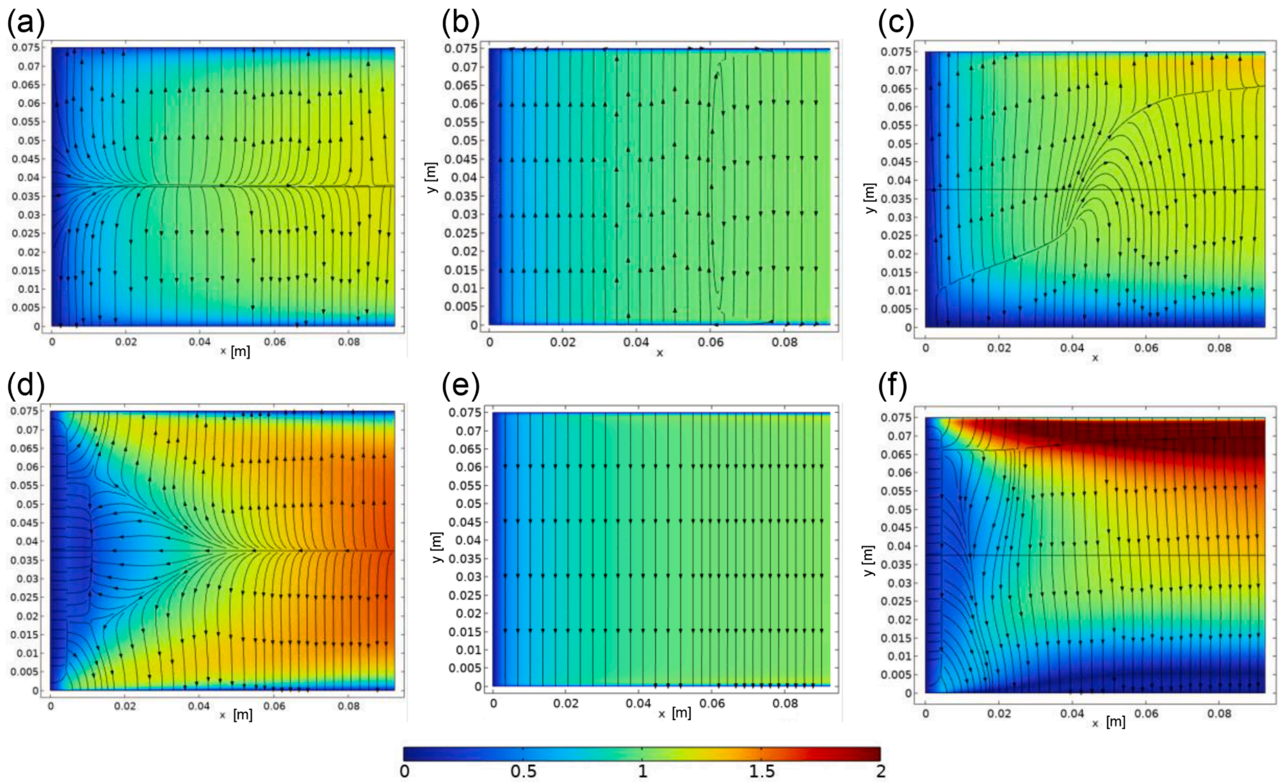

Fig. 7. The density maps illustrate the distributions of surface velocity, in m/s, with flow directed from left to right, while the lines represent the electrical current vector field. Results are shown for chutes with electrically insulating (a-c) and perfectly electrically conductive (d-f) walls under three different magnetic field configurations: (a,d) a purely toroidal magnetic field with amplitude $B_t = 0.5\,\mathrm{T}$; (b,e) a purely plate-normal magnetic field with amplitude $B_n = 0.05\,\mathrm{T}$; (c,f) an inclined magnetic field containing both toroidal and plate-normal components.

Fig. 9 show the pressure fields on the open surface. We know that the actual pressure on the open surface is zero, so the values shown in these figures can be interpreted as a measure of the surface deformation (with the deformation amplitudes $h \sim \Delta p/(\rho g \cos\beta)$). For instance, one can immediately observe that the pressure magnitude obtained for the calculations with perfectly conductive walls is at least one order of magnitude higher, indicating stronger interface deformation in this case. Indeed, if the walls are electrically conductive, then $\Delta p \sim 1000\,\mathrm{Pa}$, which corresponds to an interface deformation on the order of $\sim$20 cm, clearly indicating overflooding issue. If the walls are electrically insulating, the interface deformation is on the order of $\sim$2 cm. These predictions are in somewhat agreement with the data reported in Fig. 4b

The steady-state pressure distributions shown in Fig. 9 are influenced by the outlet boundary conditions. A pressure gradient (and the corresponding interface deformation) is required to maintain a steady flow at the prescribed flow rate, thereby reflecting the braking effect of the magnetic field. So strong pressure variations clearly indicate that the current model cannot accurately represent the flow, as it is applicable only when the free-surface deformation remains smaller than the film thickness. Nevertheless, the results obtained with this model are quick and easy to produce and still offer some predictive value, which is why we include them. The applicability of the results improves farther from the nozzle.

To relate the observations of this section to the previous analytical results, we note that the flow field near the side walls is strongly influenced by the walls themselves, and in this region the flow is three-dimensional. However, even in the case of an inclined magnetic field, the flow profile and current distribution in the middle section remain consistent with the expectations of two-dimensional flow, whose dynamics are primarily determined by the plate-normal component of the magnetic field. Indeed, in this region, the current distribution resembles that imposed by a plate-normal magnetic field, with isolines parallel to the plate.

4.2. 2D analysis of the flow with a deformable open surface

To investigate the pile-up phenomenon, we performed 2D modelling of a liquid layer with a deformable free surface, using COMSOL, tracking its shape using the phase-field method (taking the surface tension effect into account). Similar simulations were also performed in OpenFOAM using the VOF method to track the free-surface dynamics. The results obtained with OpenFOAM and COMSOL were consistent.

For these simulations, we assume that the magnetic field has only one normal component. We also assume that the plate is perfectly electrically conducting, which means that the electric field is equal zero and the current density has only one component which value is $j_z = \sigma B_n u_x$. The Lorentz force is added to the model as a body force, $\overrightarrow{f} = H(-\sigma B_n^2 u_x, 0, 0)$, where $H = 0$ in the vacuum domain and $H = 1$ in the liquid domain, and u_x is the streamwise component of the fluid velocity.

All diffuse-interface approaches introduce two fluids: in our case, lithium and a fictitious second fluid referred to as “vacuum.” The vacuum is modelled with the properties of air; however, we also examined the influence of the second fluid’s properties (such as density and viscosity) on the lithium flow. We found that when the second fluid has the properties of air, its effect on the lithium flow is negligible. For simplicity, the contact angle is set to 90°.

The numerical calculations were conducted using a uniform mesh with typically 80 grid points across the nozzle height (3.75×10^{-5} m). Higher-resolution runs (with 100 grid points) indicate some features of wavy dynamics, first appearing along the collector’s slope, but key quantities such as the mean flow velocity and the mean thickness of the liquid-metal layer remained the same. The height of the computational domain was chosen such that it does not influence the dynamics of the

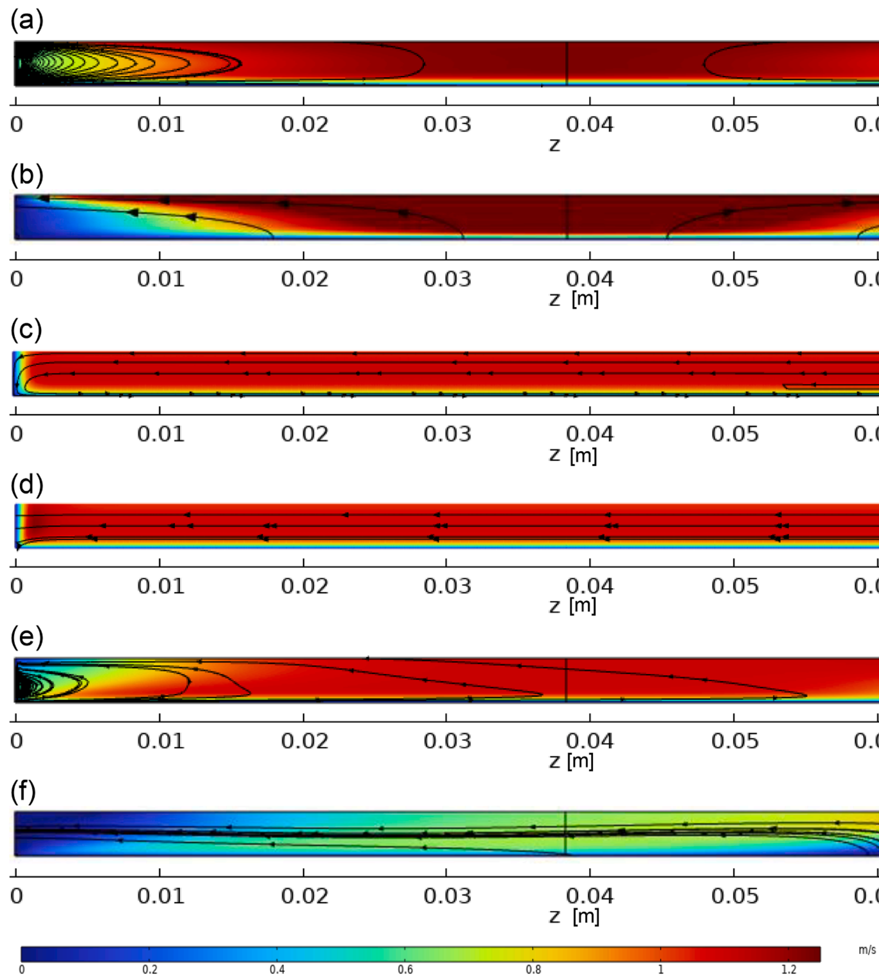

Fig. 8. The density map illustrates the velocity field, while the lines represent the electrical current. The plate's exit is shown (the vertical scale is not included, but the height of the computational domain is 3 mm). Results are presented for a purely toroidal magnetic field, $B_t = 0.5$ T (a, b); for a purely plate-normal magnetic field, $B_n = 0.05$ T (c, d); and for an inclined magnetic field with components $B_t = 0.5$ Tand $B_n = 0.05$ T (e, f). The chute is shown with electrically insulating walls (a, c, e) and perfectly electrically conducting walls (b, d, f).

free interface. Again, different domain heights were tested to verify this.

The transient simulations were performed using an initial condition corresponding to stationary fluids, with the film thickness set equal to the nozzle thickness.

In these 2D simulations, the flat plate is extended by adding two components that schematically represent a compression nozzle and a collector (see Fig. 10). For the nozzle, a channel with a fixed height equal to the nozzle height is introduced, and inlet boundary conditions—specifically, a uniform velocity profile—are applied at the nozzle entrance. For the collector, a unit with a sliding surface and an outlet is included. Although the design of a real collector is more complex, in this study we represent the 3D collector with a simplified 2D geometry, focusing primarily on the outlet's flow area, which is approximately twice that of the nozzle and consistent with the configuration used in the experimental setup. Furthermore, we later demonstrate that, in this case, the key flow features are governed by the design of the experimental chute rather than by the collector. At the collector's exit, a zero-pressure boundary condition is applied. The vertical boundaries confining the second liquid are modeled as impermeable walls, while the top boundary is also assigned a zero-pressure condition. The entire geometry described above is inclined at 5° relative to gravity.

Fig. 10 illustrates the flow pattern for an inlet flow rate of 72 g/s (inlet velocity of 64 cm/s) when the magnetic field is switched off. Small-amplitude waves can be observed forming on the free surface as the liquid descends along the collector.[2] It is important to note that the numerical resolution used in this simulation is insufficient to obtain accurate results that would resolve the turbulent nature of the flow. Nevertheless, the governing equations that we solve still conserve mass and momentum, thus offering a reasonable approximation of the flow characteristics. To support this, Fig. 11 presents the results obtained using two different resolutions, where one can see that although the finer details of the flow vary with resolution, the overall flow features remain consistent.

Next, the magnetic field is switched on, producing a piling-up effect (see Fig. 12). In particular, Fig. 12b shows that the jet flow is lifted from the surface and rapidly dispersed due to the strong action of the magnetic field, illustrating the quick establishment of the gravity-driven flow. It is also worth noting that the disintegration of the jet occurs at a distance of about 2 cm, which aligns with our simple estimate based on the product of the inlet velocity and breaking time, $U_0\tau_b = U_0\frac{1}{Ha_n^2}\frac{h_0^2}{\nu} =$

[2] By introducing a small imperfection at the nozzle (e.g., a bump on the plate near the nozzle), it is possible to induce larger surface waves, which develop as they travel along the plate. These results are not shown in this work.

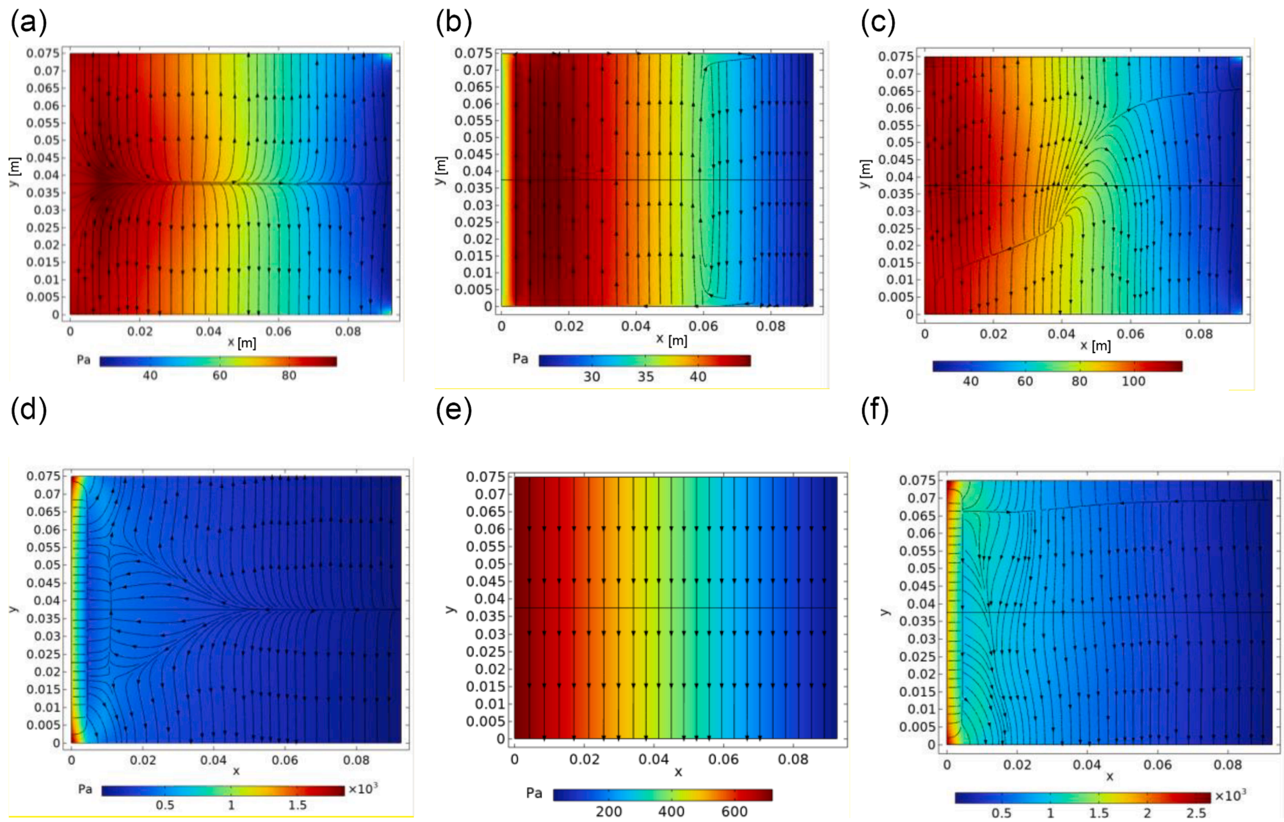

Fig. 9. Pressure distributions (in Pa) on the open surface obtained from the calculations with fixed thickness and with stress-free boundary condition applied at the free surface. The flow proceeds from left to right. The lines represent the electrical current vector field. Results are shown for chutes with electrically insulating (a-c) and perfectly electrically conductive (d-f) walls under three different magnetic field configurations: (a,d) a purely toroidal magnetic field with amplitude $B_t = 0.5$ T; (b,e) a purely plate-normal magnetic field with amplitude $B_n = 0.05$ T; (c,f) an inclined magnetic field containing both toroidal and plate-normal components.

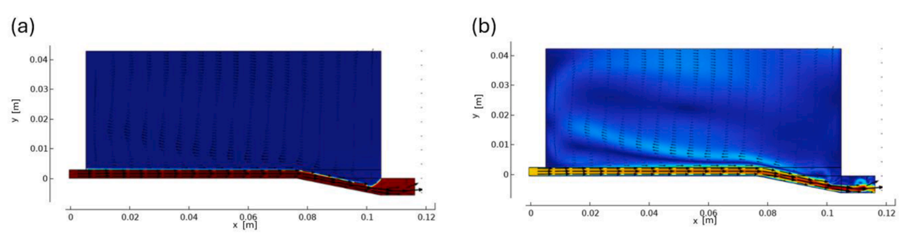

Fig. 10. 2D modelling of an open-surface flow of a liquid metal along the midplane of an experimental module. No magnetic field is applied. Steady-state shape of an open surface (a), and velocity field (b) are shown. The inlet velocity is 64 cm/s.

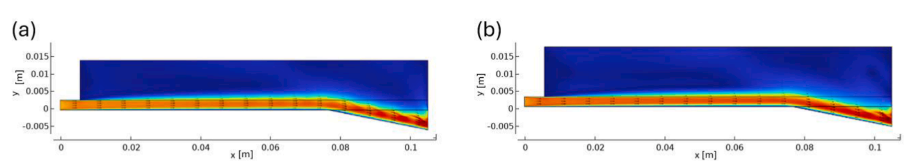

Fig. 11. Velocity fields are presented for the case without an imposed magnetic field, at two resolutions: 3.75×10^{-5} m (a) and 7.5×10^{-5} m (b).

L_{magn}.

An interesting observation from Fig. 12a is that the flow pattern cannot, in fact, be divided into distinct regions dominated separately by inertia and gravity. In the steady state, the entire module is uniformly flooded, with a fast jet flow developing near the bottom of the liquid metal pool. The surface velocity remains low and approaches zero in the region close to the nozzle. As a result, there is general qualitative agreement between Figs. 12 and 4; however, the agreement is not exact. The actual flow is more complex than the stepwise transition from inertia-driven to gravity-driven behaviour: flooding of the region upstream of the step slightly reduces the predictions reported in Fig. 4.

In Fig. 13, one can see that at the initial stages, pushing the fluid onto the plate does produce a “bump,” which could be interpreted as the boundary between inertia-driven and gravity-driven flows. However, a high sharp boundary separating the flow regimes is unstable, and its collapse (as also observed in the experimental images shown in [17], however, through development of 3D instabilities not considered here) results in even flooding of an entire experimental module.

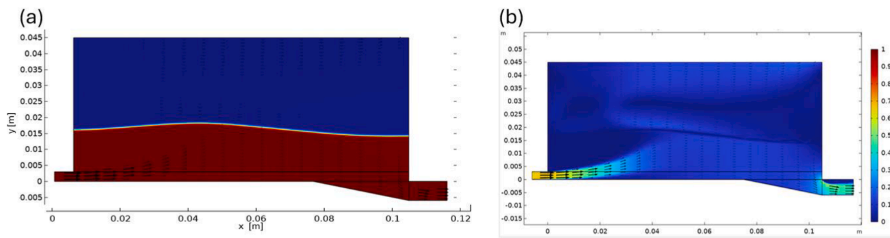

Fig. 12. Snapshots of the free surface and velocity field at $t = 2$ s (at the initial moment, the plate is covered by a stationary film of uniform thickness of 3 mm). The inlet velocity is 64 cm/s, and the magnetic field is oriented normal to the plate with a magnitude of 0.05 T.

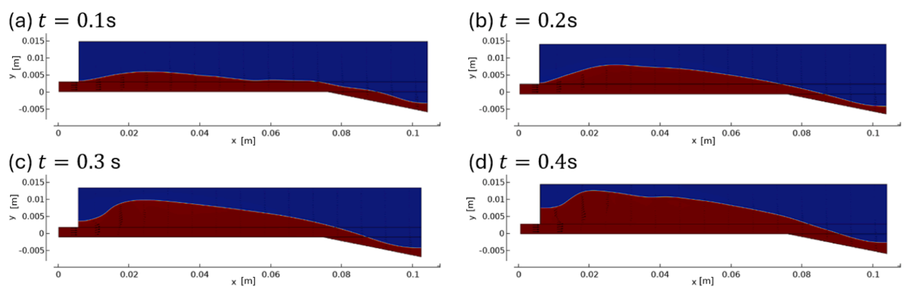

Fig. 13. Shapes of an open surface after the magnetic field is switched on.

One may argue whether the uniform flooding results from the limited flow rate imposed by the collector design or from the disruption of the flow by the plate itself. Fig. 14 illustrates the results obtained when the entire right boundary of the computational domain is modeled as an outlet flow (no back wall). Even in this case, at the steady-state, the module becomes evenly flooded, indicating that the true cause is the braking effect to the flow associated with the plate.

The results shown in Fig. 14 were obtained with an inlet flow speed of 1.28 m/s for a plate of double length, with the expectation of producing a region of fast surface flow near the nozzle. However, the results indicate that this was not achieved.

5. Conclusions

In this work, we discuss the key features of open-surface flow of an electrically conducting fluid down an inclined electrically conductive plate in the presence of a magnetic field. The study supports the design of an experimental module and is therefore focused on parameters expected in the experiment, including a relatively short and wide chute and a thin fluid film. We do not present the results of direct 3D modelling of the experimental module here, as these will be reported in a separate publication.[3] Instead, the aim of this work is to highlight more fundamental observations across a wide range of parameters that can inform the design of any fast-flow, open-surface experiment.

The flow down the chute transitions from inertia-driven flow (with parameters defined by the inlet conditions) to gravity-driven flow (which develops at some distance from the nozzle and whose parameters are independent of the initial thickness and velocity). This transition requires a very long chute if no magnetic field is applied, in which case only inertia-driven flow would be observed. In the presence of a magnetic field, however, the transition is likely to complete within the experimental chute. Furthermore, the steady-state flow may also be influenced by the collector's capacity.

The open-surface film flow down an inclined chute is susceptible to hydrodynamic instabilities. A strong magnetic field, however, can effectively suppress these instabilities, leading to laminarization of the flow and the reduction of surface waves. In the presence of a magnetic field, a laminar flow is therefore expected, which is the focus of the current study.

Additionally, because the chute is wide and the liquid layer is thin, the effect of the plate-normal magnetic field on the flow is considered strong. This allows us to focus on the analysis of a 2D geometry that represents the flow in the middle of the chute, at some distance from the side walls. For this 2D geometry, we developed analytical equations describing the characteristics of gravity-driven flow, and next by applying mass balance, we can also draw conclusions about the transition from inertia-driven to gravity-driven flow.

In particular, it was found that an experimental module with highly electrically conductive walls (as in the designed experiment) is susceptible to overflooding when either the magnetic field is strong or the inlet velocity is high. The limiting parameters will be experimentally assessed and compared with the predictions of this work. Furthermore, in the case of an electrically conductive chute, increasing the fluid supply at the top of the plate does not accelerate the flow; instead, it results in additional piling up. The flow velocity along the chute can be controlled only by the inclination angle and the magnetic field.

We also conducted numerical modeling of the flow using two different approaches. In the first model, we developed a 3D solution that neglects deformation of the free surface. This analysis shows that the side walls exert a strong influence, with the flow significantly affected at distances of several layer thicknesses from the walls. Moreover, introducing a normal component to the magnetic field creates asymmetry in the flow pattern, which may cause the fluid to detach from one of the side walls. At the same time, a region of essentially 2D flow can be always identified in the central portion of the plate.

Finally, we performed 2D modelling of the flow (focused on the centre of the plate) using the phase-field approach to trace the shape of the free surface. The numerical results confirm the overflooding predictions. However, they also show that the flow structure cannot be reduced to a simple separation between fast, inertia-driven flow and slower, gravity-driven flow. Instead, we observed uniform flooding

[3] The results of the ANSYS-based CFD analysis will be reported in two publications: *Three-Dimensional Computational Analysis of a Liquid-Lithium Divertor Experiment* by Deepa Gupta et al. and *Magnetohydrodynamic Analysis of a Liquid-Lithium Divertor Experiment* by Andrei Khodak et al. These works are being prepared for the TOFE 2026 conference, with subsequent publications planned in *Fusion Science and Technology*.

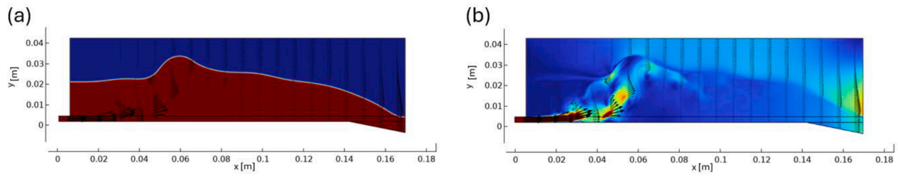

Fig. 14. Snapshots of the free surface and velocity at $t = 2$ s (at the initial moment, the plate is evenly covered with a liquid film 3 mm deep). The results were obtained for a plate 18.5 cm in length with an inlet velocity of 1.28 m/s.

across the entire chute, which resembles a pool filled with liquid metal. The surface velocity of the liquid metal remains relatively low, while faster flow occurs only at certain depths within the pool.

The overall conclusions of this analysis indicate that the targeted flow parameters can be achieved with this module design when the magnetic field is absent or relatively weak. For the chute with highly electrically conductive walls, the presence of a strong magnetic field is expected to cause flooding, which may escalate to overflooding in the case of excessively strong flow. A flooded chute does not display the features of the fast-flow concept, exhibiting relatively low surface velocity along the entire chute. The flow speed cannot be improved by increasing the throughput flow rate. The lower flow rates of the gravity-driven flow are primarily responsible for the module's inability to transport the liquid effectively.

Once experimentally validated, the modeling methodologies employed will be applied to PFC module designs that incorporate features such as electrically non-conductive walls to mitigate MHD-induced pile-up. The replaceable module design allows modification of its features, with the utimate objective of achieving steady open-surface lithium flow within an operational fusion device. We believe that the proposed experimental design and modeling represent an important step toward the development and implementation of liquid metal divertor technology in fusion power plants.

CRediT authorship contribution statement

A. Vorobev: Writing – original draft, Visualization, Validation, Methodology, Investigation, Formal analysis, Conceptualization. **S. Smolentsev:** Methodology, Investigation, Formal analysis. **A. Khodak:** Investigation, Formal analysis. **D. Gupta:** Investigation, Formal analysis. **D. Suarez:** Investigation, Formal analysis. **D. O'Dea:** Formal analysis, Data curation. **G. Stoneham:** Formal analysis, Data curation, Conceptualization. **A. Shone:** Project administration, Conceptualization. **K. Moshkunov:** Conceptualization.

Declaration of competing interest

The authors declare the following financial interests/personal relationships which may be considered as potential competing interests. Anatoliy Vorobev reports financial support was provided by US Department of Energy. Sergey Smolentsev reports financial support was provided by US Department of Energy. Andrei Khodak reports financial support was provided by US Department of Energy. Deepa Gupta reports financial support was provided by US Department of Energy. Daniel Suarez reports financial support was provided by US Department of Energy. Daniel O'Dea reports financial support was provided by US Department of Energy. George Stoneham reports financial support was provided by US Department of Energy. Andrew Shone reports financial support was provided by US Department of Energy. Konstantin Moshkunov reports financial support was provided by US Department of Energy. If there are other authors, they declare that they have no known competing financial interests or personal relationships that could have appeared to influence the work reported in this paper.

Acknowledgements

This work was undertaken as part of the Milestone-based Fusion Development Program. We would also like to thank Dr. Robin Kamenicky for the thorough internal review of the manuscript, as well as Dr. Samara Levine from materials data, and the UIUC team supervised by Prof. D. Andruczyk for their assistance with the lithium loop design.

Appendix

Here we derive expressions (9) and (10), which describe the steady plane-parallel flow of an electrically conductive liquid down an inclined plate in the presence of a magnetic field normal to the plate.

For this derivation, we use the MHD equations written under the quasi-static approximation, where the total magnetic field is represented as $\vec{B} = \vec{B}_0 + Re_m \vec{B}_1$, with $\vec{B}_0$ being the constant externally applied magnetic field, and $Re_m \vec{B}_1$, the small induced magnetic field. Here, $Re_m = \frac{U_0 h_0}{\nu_m} \ll 1$ is the magnetic Reynolds number, and the magnetic diffusivity is $\nu_m = \frac{1}{\mu_0 \sigma}$ (the magnetic constant $\mu_0 = 4\pi \cdot 10^{-7} \frac{N}{m}$, and σ is the electrical conductivity of the liquid metal).

The non-dimensional form of the MHD equations under this approximation is expressed as follows:

$$\nabla \cdot \vec{u} = 0, \nabla \cdot \vec{B}_1 = 0, \tag{A1}$$

$$\nabla^2 \vec{B}_1 = -\left(\vec{B}_0 \cdot \nabla\right) \vec{u}, \tag{A2}$$

$$\frac{\partial \vec{u}}{\partial t} + (\vec{u} \cdot \nabla) \vec{u} = -\nabla \Pi + N\left(\vec{B}_0 \cdot \nabla\right) \vec{B}_1 + \frac{1}{Re} \nabla^2 \vec{u}, \tag{A3}$$

$$\Pi = p + N\left(\vec{B}_0 \cdot \vec{B}_1\right) + \frac{1}{Fr^2} (\vec{\gamma} \cdot \vec{r}). \tag{A4}$$

Here, $\vec{u}$ and p denote the fluid velocity and pressure, $\vec{\gamma}$ is the upward-directed unit vector, and $\vec{r}$ is the position vector.

Eqs. (A1)–(A4) are obtained using the following characteristic scales: h_0, U_0, h_0/U_0, ρU_0^2, and B_0 for length, velocity, time, pressure, and magnetic field, respectively. Here, h_0 is the thickness of a liquid metal film, $U_0 = \frac{Q}{Wh_0}$ is the mean velocity, where Q is the volumetric flow rate and W is the width of the liquid layer. The equations include three non-dimensional parameters,

$$Re = \frac{U_0 h_0}{\nu}, Fr = \frac{U_0}{\sqrt{gh_0}}, N = \frac{\sigma B_0^2 h_0}{\rho U_0}, \tag{A5}$$

which are the Reynolds number, the Froude number, and the magnetic interaction number.

We restrict this derivation to a steady, plane-parallel flow, in which the velocity and induced magnetic field vectors possess the following symmetries: $\vec{u} = (u_x(y), 0, 0)$ and $\vec{B}_1 = (B_{1x}(y), 0, 0)$, where y is the coordinate that is normal to the plate. The flow is subjected to a constant plate-normal magnetic field, $\vec{B}_0 = (0, 1, 0)$. As for any other plane-parallel flow, the continuity equation is automatically satisfied (and, similarly, the Gauss's law for the magnetic field is also automatically satisfied). The non-linear term in the Navier-Stokes equation vanishes. As a result, the remaining equations from the set (A1)–(A4) reduce to the following:

$$\frac{\partial^2 B_1}{\partial y^2} = -\frac{\partial u_x}{\partial y}, \tag{A6}$$

$$0 = -\frac{\partial \Pi}{\partial x} + N\frac{\partial B_{1x}}{\partial y} + \frac{1}{Re}\frac{\partial^2 u_x}{\partial y^2}, \tag{A7}$$

$$\Pi = p + \frac{1}{Fr^2}(-x\sin\beta + y\cos\beta). \tag{A8}$$

These differential equations must be supplemented with the following boundary conditions:

$$y = 0 : u_x = 0, B_{1x} = \kappa\frac{\partial B_{1x}}{\partial y} \tag{A9}$$

$$y = 1 : \frac{\partial u_x}{\partial y} = 0, B_{1x} = 0. \tag{A10}$$

The first line (A9) specifies the conditions on the plate, consisting of the standard no-slip boundary condition and a mixed boundary condition for the induced magnetic field that incorporates the conductance κ, reflecting the finite electrical conductivity of the substrate. The second line (A10) defines the boundary conditions at the open surface—namely, the stress-free condition for the velocity field and the requirement that the open surface is electrically insulating.

Using Eq. (A6), the boundary conditions (A9) and (A10), and the relation $\int_0^1 u_x \mathrm{d}y = 1$, one obtains that

$$B_{1x} = -\int_0^y u_x \mathrm{d}y + \frac{y+\kappa}{1+\kappa}. \tag{A11}$$

The electric current density is given by $\vec{j} = \nabla \times \vec{B}_1$, which shows that the electric current flows in the spanwise direction,

$$j_z = -\frac{\partial B_{1x}}{\partial y} = u_x - \frac{1}{1+\kappa} \tag{A12}$$

In case of an electrically insulating plate ($\kappa = 0$), $j_z = u_x - 1$ and the total current satisfies $\int_0^1 j_z \mathrm{d}y = 0$. In contrast, for a perfectly conducting plate ($\kappa = \infty$), $j_z = u_x$, and the total current in the liquid volume is non-zero, as the electrical circuit closes through the current flowing within the solid plate.

Substituting (A11) into (A7), one obtains

$$0 = -\frac{\partial \Pi}{\partial x} + N\left(-u_x + \frac{1}{1+\kappa}\right) + \frac{1}{Re}\frac{\partial^2 u_x}{\partial y^2}. \tag{A13}$$

Next, let us assume that the fluid can be pushed onto the substrate (so the streamwise pressure difference is formed, $\frac{\partial p}{\partial x} \equiv -A$) and that the fluid motion is also driven by gravity. Hence,

$$\frac{\partial \Pi}{\partial x} = -A - \frac{\sin\beta}{Fr^2}. \tag{A14}$$

Substituting (A14) into (A13), integrating twice, and applying the boundary conditions, one obtains,

$$u_x = \frac{1}{N}\left(A + \frac{\sin\beta}{Fr^2}\right)(1 - \cosh Ha y + \tanh Ha \sinh Ha y). \tag{A15}$$

Using the relation $\int_0^1 u_x \mathrm{d}y = 1$, one obtains Eqs. (9) and (10).

Data availability

No data was used for the research described in the article.

References

[1] L.E. Zakharov, What can and cannot be expected from tokamak fusion, At. Energy 130 (2021) 94–103.

[2] A. de Castro, C. Moynihan, S. Stemmley, M. Szott, D.N Ruzic, Lithium, a path to make fusion energy affordable, Phys. Plasmas 28 (2021) 050901.

[3] G. Zuo, et al., Results from an improved flowing liquid lithium limiter with increased flow uniformity in high power plasmas in EAST, Nucl. Fusion 59 (2019) 016009.

[4] S. Smolentsev, T. Rognlien, M. Tillack, L. Waganer, C. Kessel, Integrated liquid metal flowing first wall and open-surface divertor for Fusion Nuclear Science Facility: concept, design, and analysis, Fusion Sci. Technol. 75 (2019) 939–958.

[5] S. Smolentsev, Design window for open-surface lithium divertor with helium-cooled substrate, Fusion Eng. Des. 173 (2021) 112930.

[6] A. Bhattacharya, S.J. Zinkle, J. Henry, S.M. Levine, P.D. Edmondson, M.R. Gilbert, H. Tanigawa, C.E. Kessel, Irradiation damage concurrent challenges with RAFM and ODS steels for fusion reactor first wall/blanket: a review, J. Phys. Energy 4 (2022) 034003.

[7] S.J. Zinkle, H. Matsui, D.L. Smith, A.F. Rowcli, E. van Osch, K. Abe, V.A. Kazakov, Research and development on vanadium alloys for fusion applications, J. Nucl. Mater. 258-263 (1998) 205–214.

[8] S. Nogami, et al., Neutron irradiation tolerance of potassium-doped and rhenium-alloyed tungsten, J. Nucl. Mater. 553 (2021) 153009.

[9] T. Eich, et al., Scaling of the tokamak near the scrape-off layer H-mode power width and implications for ITER, Nucl. Fusion 53 (2013) 093031.

[10] V.V. Baranov, I.A. Evtushchenko, I.R. Kirillov, E.V. Firsova, V.V. Yakovlev, Liquid metal film flow for fusion application, Magnetohydrodynamics 30 (1994) 460–467.

[11] S. Molokov, C.B. Reed, *Review of free-surface MHD experiments and modeling*, Argonne National Laboratory technical report, ANL/'TD/TM99-O8, 2000.

[12] A. Oron, S.H. Davis, S.G. Bankoff, Long-scale evolution of thin liquid films, Rev. Mod. Phys. 69 (1997) 931–980.

[13] B.-Q. Liu, J.-C. Yang, T.-Y. Qi, D.-W. Ren, J. Zhang, M.-J. Ni, Experimental study on the lithium film flow in the spanwise magnetic field, Fusion Eng. Des. 136 (2018) 522–526.

[14] E. Platacis, A. Flerov, A. Klukin, S. Ivanov, A. Sobolevs, A. Shishko, L. Zaharov, M. Gryaznevich, Gravitational flow of a thin film of liquid metal in a strong magnetic field, Fusion Eng. Des. 89 (2014) 2937–2945.

[15] P.P. Vieweg, Y. Kolesnikov, C. Karcher, Experimental study of a liquid metal film flow in a streamwise magnetic field, Magnetohydrodynamics 58 (2022) 5–11.

[16] K. Itoh, Y. Tsuji, H. Nakamura, Y. Kukita, Initial free surface instabilities on a high-speed water jet simulating a liquid-metal target, Fusion Technol. 36 (1999) 69–84.

[17] M. Narula, M.A. Abdou, A. Ying, N.B. Morley, M. Ni, R. Miraghaie, J. Burris, Exploring liquid metal plasma facing component (PFC) concepts—Liquid metal film flow behavior under fusion relevant magnetic fields, Fusion Eng. Des. 81 (2006) 1543–1548.

[18] J.-C. Yang, T.-Y. Qi, M.-J. Ni, Z.-H. Wang, Flow patterns of GaInSn liquid on inclined stainless steel plate under a range of magnetic field, Fusion Eng. Des. 109-111 (2016) 861–865.

[19] A.Y. Ying, et al., Exploratory studies of flowing liquid metal divertor options for fusion-relevant magnetic fields in the MTOR facility, Fusion Eng. Des. 72 (2004) 35–62.

[20] X. Zhang, C. Pan, Z. Xu, MHD stability analysis and flow controls of liquid metal free surface film flows as fusion reactor pfcs, Plasma Sci. Technol. 18 (2016) 1204–1214.

[21] G.Y. Antar, et al., Plasma–lithium interaction in the CDX-U spherical torus, Fusion Eng. Des. 60 (2002) 157–166.

[22] K. Miyazaki, S. Inoue, N. Yamaoka, T. Horiba, K. Yokomizo, Magneto-hydro-dynamic pressure drop of lithium flow in rectangular ducts, Fusion Technol. 10 (1986) 830–836.

[23] A.Y. Shishko, A theoretical investigation of steady-state film flow in a coplanar magnetic field, Magnetohydrodynamics 2 (1992) 75–88.

[24] H.W. Davison, Compilation of Thermophysical Properties of Liquid Lithium, NASA Scientific and Technical Publications, 1968.

[25] C.-S. Yih, Stability of a liquid flow down an inclined plane, Phys. Fluids 6 (1963) 321–334.

[26] D.Y. Hsieh, Stability of a conducting fluid flowing down an inclined plane in the presence of a magnetic field, Phys. Fluids 8 (1965) 1785–1791.

[27] D. Suarez, S. Smolentsev, Development of three simulation tools for open-surface liquid metal magnetohydrodynamic flows in plasma-facing components using OpenFOAM, Fusion Eng. Des. 215 (2025) 115008.

[28] S.A. Krat, A.S. Popkov, Y.M. Gasparyan, A.A. Pisarev, P. Fiflis, M. Szott, M. Christenson, K. Kalathiparambil, D.N. Ruzic, Wetting properties of liquid lithium on lithium compounds, Fusion Eng. Des. 117 (2017) 199–203.

[29] J.-H. Pan, M.-J. Ni, Magnetohydrodynamic effects on liquid metal flows in an open channel for fusion plasma facing components with a transverse magnetic field, Nucl. Fusion 65 (2025) 046015.

[30] F. Saenz, A.E. Fisher, J. Al-Salami, B. Wynne, Z. Sun, T. Tanaka, T. Kunugi, J. Yagi, K. Kusumi, Y. Wu, G. Yamazaki, C. Hu, K. Hanada, E. Kolemen, Experimental, numerical and analytical evaluation of j×B-thrust for fast-liquid-metal-flow divertor systems of nuclear fusion devices, Nucl. Fusion 63 (2023) 096015.